Journal of Membrane Science 448 (2013) 81–92

Contents lists available at ScienceDirect

Journal of Membrane Science

journal homepage: www.elsevier.com/locate/memsci

Synergetic effects of oxidized carbon nanotubes and graphene oxide on fouling control and anti-fouling mechanism of polyvinylidene fluoride ultrafiltration membranes

Jiguo Zhang [a], Zhiwei Xu [a,*], Mingjing Shan [a], Baoming Zhou [a], Yinglin Li [a], Baodong Li [b], Jiarong Niu [b], Xiaoming Qian [b,**]

[a] State Key Laboratory of Hollow Fiber Membrane Materials and Processes, Tianjin Polytechnic University, Tianjin 300387, People's Republic of China
[b] School of Textiles, Tianjin Polytechnic University, Tianjin 300387, People's Republic of China

ARTICLE INFO

Article history:
Received 29 May 2013
Received in revised form
25 July 2013
Accepted 26 July 2013
Available online 7 August 2013

Keywords:
Synergetic effects
Graphene oxide and oxidized carbon nanotubes
Permeability
Anti-fouling performance
Ultrafiltration membranes

ABSTRACT

This study investigated the remarkable synergetic effect between two-dimensional graphene oxide (GO) and one-dimensional oxidized carbon nanotubes (OMWCNTs) on permeation and anti-fouling performance of polyvinylidene fluoride (PVDF) composite membranes. Stacking of individual GO is effectively inhibited by introducing OMWCNTs. Long and tortuous OMWCNTs can bridge adjacent GO and inhibit their aggregation, which makes the materials achieve their highest potential for improving the anti-fouling performance of composite membranes. Ultraviolet–visible spectra and zeta potential study well demonstrated that the dispersion of hybrid materials is better than that of either GO or OMWCNTs. The morphology of different membranes demonstrated that modified membranes have bigger pore density, which undoubtedly played a positive role in permeation flux. Compared with the pristine PVDF (78°), the hydrophilicity of membranes with the ratio of 1:9 (GO/OMWCNTs) showed a marked improvement (52.5°) in contact angle. With a GO/OMWCNTs ratio of 5:5, the pure water flux is enhanced by 251.73% compared with pristine PVDF membranes, while improved by 103.54% and 85.68% for the PVDF/OMWCNTs and PVDF/GO membranes, respectively. The membrane fouling mechanism was studied by resistance-in-series model, and results indicated that membranes tended to be fouled by the cake layer. Additionally, an atomic force microscope (AFM) analysis with a BSA-immobilized tip indicated low adhesion force with the modified membranes, while the pristine PVDF membranes exhibited strong adhesion to the probe, consistent with the fouling properties of the membranes. The newly-developed modified membranes, especially the PVDF/GO/OMWCNTs membranes, demonstrated an impressive prospect for the anti-irreversible fouling performance in dead end filtration experiments. And the pure water flux recovery achieved 98.28% for membranes with the ratio of 5:5 (GO/OMWCNTs), which contributing to the synergistic effect of the hybrid samples. As a result, the optimum ratio of GO/OMWCNTs immobilizing membranes for ultrafiltration membrane application in terms of highest permeability and lowest fouling was 5:5. Conspicuously, the ease of synthesis and the exceptional permeability and anti-fouling performance render that the low-dimensional carbon nanomaterial modification is an attractive way of designing future ultrafiltration membranes in both conventional fields and new emerging areas.

1. Introduction

Despite its high hydrophobicity, poly (vinylidene fluoride) (PVDF) is still a popular membrane material due to its good chemical resistance, thermal stability and mechanical properties [1–3]. Nevertheless, PVDF membrane fouling results in substantial flux decline that necessitates frequent membrane cleaning and replacement. Consequently, efficient application of membrane technology in wastewater reclamation is significantly hampered by the phenomenon of organic fouling as wastewater effluent contains a considerable amount of organic substances. In recent years, in order to further reduce the susceptibility of PVDF membranes to biofouling or to enhance their anti-fouling performance, various methods to increase their surface hydrophilicity have been described, such as coating [4], adsorption [5], surface graft polymerization [6] and chemical modification of pristine PVDF [7]. Besides, blending modification is another

* Corresponding author. Tel./fax: +86 22 83955231.
** Corresponding author. Tel./fax: +86 22 83955051.
E-mail addresses: xuzhiwei@tjpu.edu.cn (Z. Xu), qianxiaoming@tjpu.edu.cn (X. Qian).

0376-7388/$ - see front matter © 2013 Elsevier B.V. All rights reserved.
http://dx.doi.org/10.1016/j.memsci.2013.07.064

practical method without any pre-treatment or post-treatment procedures [8].

In recent years, several authors have shown the successful preparation of carbon nanotubes blended polymeric composite membranes and they have mainly studied the effects of carbon nanotubes on the performance of membranes [9,10]. In addition, former reports (including our previous work), have simply investigated the effects of graphene derivatives on the performance of composite membranes [11–13]. And results indicated that introducing low-dimensional carbon nanomaterials in the membrane matrix can improve the hydrophilicity, water permeability and the anti-fouling performance of polymer based nanocomposite membranes. However, like carbon nanotubes the problem of dispersion is strongly present for graphene derivatives as well due to strong Vander Waals forces and inter-planer stacking [14–16]. Consequently, the poor dispersion of carbon nanotubes and graphene in polymeric matrices may limit the extent of realizing potential improvements of composite membranes and the performance of low-dimensional nanomaterials-based composite membranes is hampered by the aggregation and stacking of either carbon nanotubes or graphene. It is known that by bringing together two nanofillers like carbon nanotubes and graphene derivatives they form a co-supporting network of both fillers like a hybrid net structure in which the platelet geometry shields the tube fillers from fracture and damage during processing whilst still allowing full dispersion of both during high-power sonication, thus causing improved properties [17]. Hence, we can expect that integrating one-dimensional oxidized carbon nanotubes (OMWCNTs) and two-dimensional graphene oxide (GO) resulted in a strong synergistic effect between the two materials, consequently leading to a superior ultrafiltration membrane with higher anti-fouling performance compared with the membranes modified by either GO or OMWCNTs. Furthermore, as is known in the art, the synergetic effect of OMWCNTs and GO on the membrane – foulant adhesion forces and membrane-fouling behavior as well as on the anti-fouling mechanism of PVDF ultrafiltration membranes has not yet to be systematically studied. And it is an open question to completely understand the synergistic effect brought about by the nanomaterial mixture of different ratios.

Based on these considerations and the body of previous research, the objective of this work is to synthesize composite membranes of different nanofiller ratios using a non-solvent induced phase separation method and determine the synergistic effects on the fouling control and anti-fouling mechanism of two highly-potent nanomaterials in the matrix. These results offer a novel yet simple and effective way of designing composite ultrafiltration membranes with extraordinary performance by incorporating two different low-dimensional carbon nanomaterials neither one of which alone might be essentially perfect for the required applications.

2. Experimental

2.1. Materials

The PVDF (FR904) was purchased from Shanghai 3F New Materials Co. Ltd. China. N, N-dimethylacetamide (DMAc, $>99.5\%$, reagent) and polyvinyl pyrrolidone (PVP) were purchased from Tianjin Weichen Chemical Reagent Co. Ltd. China. Multi-walled carbon nanotubes (MWCNTs, with diameters of 10–50 nm and length of 1–30 μm) were obtained from Nanjing XF Nanomaterial Science and Technology Co. Ltd. The purity of received MWCNTs is 95%. Oxidized carbon nanotubes (OMWCNTs) were synthesized by the previous reports [18]. Graphite oxide powders were prepared by improved Hummers' method [19]. Then the powders were suspended in pure water (1 mg/ml) and sonicated for 2.5 h to generate a graphene oxide (GO) suspension. Subsequently, the aqueous GO suspension was frozen into an ice cube in a refrigerator (258.15 K) for 8 h and then was freeze-dried using a FD-1A-50 lyophilizer (Boyikang Co. Ltd., China) with a condenser temperature of 223.15 K at an inside pressure of less than 20 Pa. After 48 h lyophilization and 48 h vacuum drying (318.15 K) process, low-density, loosely packed GO powder was finally obtained.

2.2. Preparation of membranes

All the membranes were prepared by the classical phase inversion method using PVDF and PVP as the solute materials, DMAc as the solvent, low-dimensional carbon materials as the additive, and distilled water at room temperature as the nonsolvent coagulation bath. The different ratios of GO and OMWCNTs mixtures with a total of 1 wt% (mass of low-dimensional carbon materials/mass of polymer) were first imported into DMAc solvent, and then the solution was sonicated for 30 min (40 kHz) before the addition of PVP (1 g) and PVDF (15 g) powders. Casting solution was then mechanically stirred at 323.15 K for at least 24 h. After fully degassing, the casting solution was spread onto clean glass plates with 200 μm gap and then immersed into coagulation bath (distilled water) for 30 min. After peeling off from the glass plates, the resultant membranes were rinsed in distilled water before ultrafiltration tests.

2.3. Characterization of low-dimensional carbon nanomaterials

Ultraviolet–visible (UV–vis) absorption spectra of GO, OMWCNTs and GO/OMWCNTs were recorded with a UV-1800 spectrophotometer. Zeta potential analyses were performed using a Delsa Nano instrument and all data were measured over five times. All the samples were dispersed by ultrasonic agitation in DMAc solution at 298.15 K for 1 h before tests.

2.4. Characterization of membranes

2.4.1. Structure and functionality

The existence of OMWCNTs and GO in ultrafiltration membranes was characterized by Fourier-Transform Infrared spectroscopy (FTIR). To determine the stability of the hydrophilicity of membranes, the membranes were stirred in frequently changed pure water for 3 weeks and then dried in air. The contact angle (CA) change with the drop age of membranes was recorded by a water contact angle system (JC2000D2). Five different points of every sample were measured and the CA was the average of these measurements.

Permeation flux of the membranes was measured by ultrafiltration experimental equipments. The sample membranes were immersed in pure water before measurement. The measuring protocol was depicted as follows: for the first 30 min, the membranes were compacted at 0.1 MPa to get a steady flux; then the flux was recorded at 0.1 MPa every 5 min, and at least 5 readings were collected to obtain an average value. The permeation flux was defined using the following Eq. (1):

$$J = \frac{Q}{AT} \tag{1}$$

where J was permeation flux of membranes for pure water ($L\,m^{-2}\,h^{-1}$), Q was volume of permeate pure water (L), A was effective area of membranes (m^2) and T was the permeation time (h).

2.4.2. Interaction force between membrane surface and AFM tip

Interaction forces between the membrane surface and a bovine serum albumin (BSA)-immobilized tip were measured by an atomic force microscope (CSPM5500). The AFM tip was modified according to the procedure described elsewhere [20]. A Si_3N_4 cantilever was treated with oxygen plasma (150 W, 60 s) and then chemically modified with 10 mM 3-aminopropyltriethox-ysilane toluene solution for 2 h at room temperature. This amine-terminated AFM tip was further reacted with glutaraldehyde (50% in H_2O) for 30 min, which was followed by reaction with the BSA in phosphate buffer solution (PBS, PH=7.4) for 40 min. Then, the tip was washed with PBS and subsequently stored in PBS.

As the membrane surface approached the BSA-immobilized AFM tip, an interaction was generated between the tip and the membrane surface, inducing a cantilever deflection. By multiplying the spring constant of the cantilever by the deflected distance (change in photodiode signals), the intermolecular force between BSA-immobilized AFM tip and membrane surface could be calculated. The force could be detected in the same manner when the surface was retracted. A force–extension curve then could be constructed from these measurements. We used a spring constant of 0.2 N m^{-1}, supplied by the manufacturer. A speed of 0.1 μm s^{-1} was applied to obtain the force–extension curves during approach and retraction of the membrane surface from the BSA-immobilized tip. All experiments were carried out in PBS at room temperature. Approximately 50 approach/retract cycles were performed for each membrane surface collected from at least five positions on the sample.

2.4.3. Fouling mechanism of membranes

In the dead-end filtration, flux decline can be caused by several factors, such as adsorption between membrane and solutions, cake or gel formation, concentration polarization, and membrane hydraulic resistance. Resistance-in-series model is particularly applicable to the analysis of flux decline of BSA [21,22]. It was described as follows:

$$J=\frac{TMP}{\mu R_{tot}} \tag{2}$$

where J is the flux (L m^{-2} h^{-1}); TMP is the transmembrane pressure (0.1 MPa); μ is the viscosity of water at room temperature (1.005×10^{-3} Pa s), and R_{tot} is the total filtration resistance.

The resistance-in-series model combines various resistances that cause flux decline as follows:

$$R_{tot}=R_m+R_g+R_c+R_a=\frac{TMP}{\mu J} \tag{3}$$

where R_m is the membrane hydraulic resistance, R_g is the cake layer resistance, R_c is the concentration polarization resistance and R_a is the adsorption resistance. And all the procedure as follows:

$$R_m=\frac{TMP}{\mu J_{mem}} \tag{4}$$

$$R_g=\frac{TMP}{\mu J_{pore}}-R_m-R_a \tag{5}$$

$$R_a=\frac{TMP}{\mu J_{irr}}-R_m \tag{6}$$

First, the membrane hydraulic resistance R_m was calculated by measuring the flux of pure water through a clean membrane (J_{mem}). After this, the fermentation broth was filtrated and the permeate flux (J_{tot}) was recorded during the whole process. According to Eq. (3), R_{tot} could be calculated during this process. Then the feed broth was replaced by pure water and the water flux in this situation J_{pore} was recorded. Subsequently, the membrane was flushed with pure water and cleaned by removing the gel layer, and then the water flux J_{irr} was determined. Thus, all membrane resistances can be quantified by Eqs. (2)–(6).

2.4.4. Anti-fouling performance of membranes

For the fouling resistance tests, pure water was first passed through the membrane until the flux remained stable over at least half an hour. The pure water flux, J_w (L m^{-2} h^{-1}), was obtained from the volume of the permeated water and then the cell was emptied and refilled with the model protein solutions comprised of 1 g l^{-1} BSA in PBS with a pH of 7.4, and the flux at each time was recorded as J_p. After BSA ultrafiltration, the fouled unit and membrane were cross-flow cleaned for 20 min with pure water at 60 min and 120 min and then refilled with pure water as a feed to determine fouling, after which water fluxes with the cleaned membranes, $J_{w,60}$ (at 60 min) and $J_{w,120}$ (at 120 min), were measured again. In order to evaluate the fouling-resistant ability of the modified membranes, the flux recovery ratio (FRR) was calculated using the following expression:

$$FRR=\frac{J_{w,60}\text{ or }J_{w,120}}{J_W}100\% \tag{7}$$

To analyze the fouling process in detail, several equations were used to describe the fouling resistance of membranes. The total flux decline ratio (DR_t), reversible flux decline ratio (DR_r), and irreversible flux decline ratio (DR_{ir}) were defined and calculated as follows:

$$DR_t=\left(1-\frac{J_p}{J_w}\right)100\% \tag{8}$$

$$DR_r=\left(\frac{J_{w,60}\text{ or }J_{w,120}-J_p}{J_w}\right)100\% \tag{9}$$

$$DR_{ir}=\left(\frac{J_w-J_{w,60}\text{ or }J_{w,120}}{J_w}\right)100\% \tag{10}$$

Obviously, DR_t is the sum of DR_r and DR_{ir}.

3. Results and discussion

3.1. UV–vis spectra and zeta potential of OMWCNTs, GO and OWMCNTs/GO

UV–vis spectra have been used for the characterization of the stabilization and dispersion of carbon nanomaterial suspension [23,24]. Fig. 1 presents the UV–vis spectra of GO suspensions, OMWCNTs suspensions and the mixture suspensions of GO and OMWCNTs. The peak in the UV–vis spectrum of GO in the region of 227–231 nm determines the degree of remaining conjugation (π–π^* transition) [16,19]. The shoulder around 300 nm can be ascribed to the n–π^* transition of carbonyl groups [19]. While almost no structural peaks can be observed in the case of OMWCNTs as shown in Fig. 1(b), which is in good agreement with the results of previous reports [25]. However, another absorption peak at 205 nm in Fig. 1(c), beside the pristine GO dispersion peak, can be seen in the mixture indicating π–π attractions between the surface of the OMWCNTs and the basal planes of GO, which further strengthened the hypothesis that the π-conjugated aromatic domains of the GO have interacted with the surface of the OMWCNTs [26]. The UV–vis results demonstrate that the suspension of OMWCNTs can be effectively stabilized using GO sheets. The ionization of oxygen groups typically leads to a high stability of GO aqueous dispersion. Considering the case of GO platelets, which are flexible in nature unlike hard disks, the interparticle

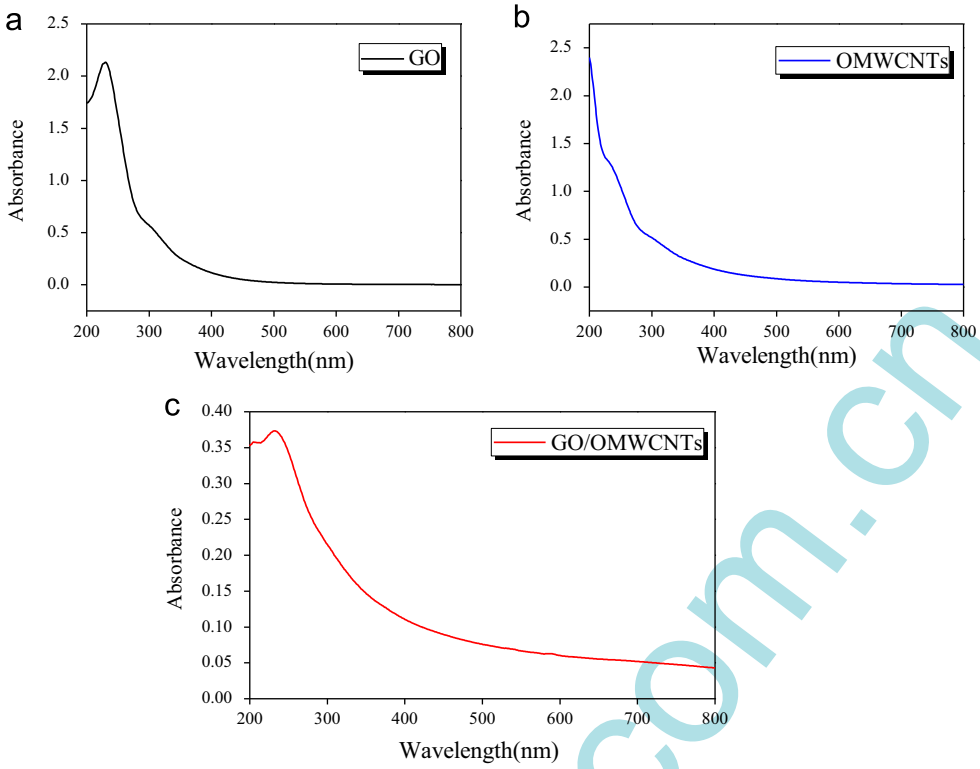

Fig. 1. UV–vis spectra of (a) GO, (b) OMWCNTs and (c) GO/OMWCNTs.

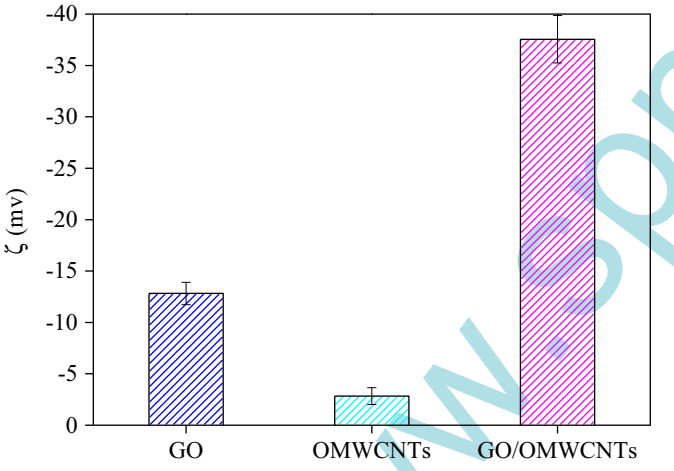

Fig. 2. Zeta potential of GO, OMWCNTs and GO/OMWCNTs.

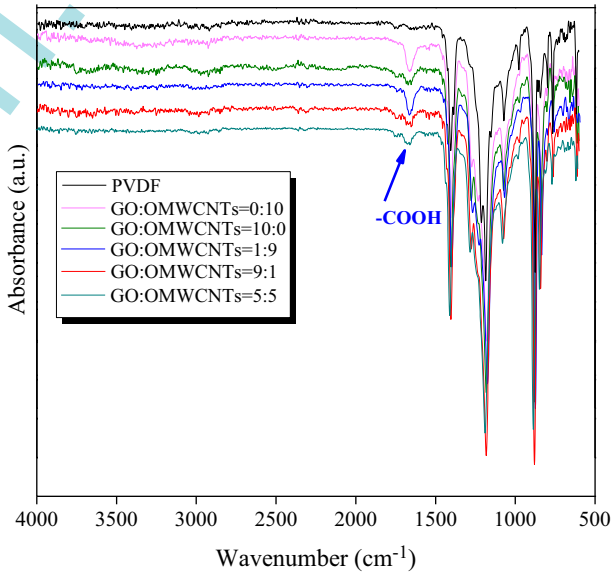

Fig. 3. FTIR spectra of pristine membranes and modified membranes.

interaction is completely based on the charge stabilization and double layer extension [27].

To better illustrate this point, zeta potential study was carried out on GO, OMWCNTs and the hybrid materials (GO/OMWCNTs). Zeta potential confers the degree of repulsion between charged particles in dispersion. Therefore, a high zeta potential is an indicator that the dispersion resists aggregation and consequently remains stable. Analysis of the zeta potential for the materials is shown in Fig. 2. The GO and OMWCNTs possessed zeta potential of -12.82 ± 1.10 mV and -2.83 ± 0.83 mV, respectively, which is consistent with previous results [26,28]. However, in the case of the hybrid materials, the zeta potential becomes significantly more negative (-37.55 ± 2.3 mV), suggesting the higher stability of mixed solution. Based on all the facts, it is concluded that the dispersion of hybrid materials is better than that of GO or OMWCNTs, causing the carbon nanomaterials fully express their potential either on the membrane surface or in the polymer matrix. It undoubtedly played a positive role in promoting membrane permeability and anti-fouling performance.

3.2. FTIR of membranes

The introduction of –COOH bonds in oxidized low-dimensional carbon nanomaterial blended PVDF membranes was confirmed by FTIR (Fig. 3), which is the main factor to improve the membrane hydrophilicity [29]. In comparison with the spectrum of pristine PVDF, the spectra of modified membranes show one new band at 1680 (–COOH). The same behavior has been observed by addition

of the OMWCNTs to the polymeric membranes [30,31]. The above results clearly demonstrated that blending the hydrophilic materials to the PVDF matrix could incorporate –COOH groups in the modified membranes and thus improve the hydrophilicity of the PVDF membranes, which has the beneficial effects for the anti-fouling performances [32].

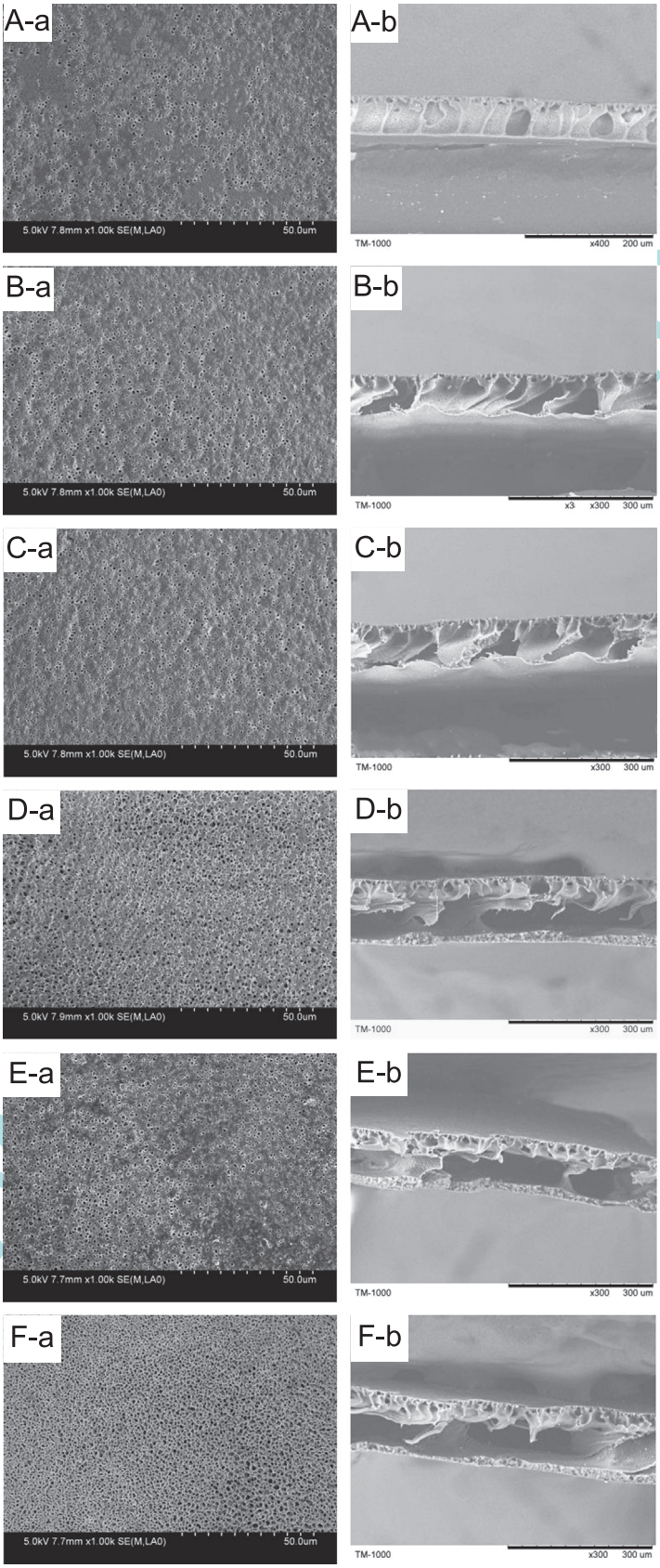

Fig. 4. (a) Surface and (b) cross-section views of (A) pristine membranes, (B) 0:10 (GO/OMWCNTs), (C) 10:0, (D) 1:9, (E) 9:1 and (F) 5:5 membranes.

3.3. Morphologies, hydrophilicity and permeability of membranes

3.3.1. Morphologies of membranes

Fig. 4 shows the SEM images of surface and cross-section (from left to right) views of the membranes. It can be seen that the introduction of carbon nanomaterials in the membranes obviously influences the pore structure. Compared with the pristine PVDF membranes, all the modified membrane surfaces exhibited denser porous structure caused by the demixing of nanomaterials during the phase inversion process [33]. Furthermore, the PVDF/GO/OMWCNTs membranes had a considerable increase of small pores and an evident improvement in surface pore density compared with PVDF/OMWCNTs or PVDF/GO membranes which could be viewed intuitively from the SEM images. In addition, the 5:5 (GO/OMWCNTs) membranes have the biggest pore density which is good for the permeation of membranes [34]. It can be explained as follows: during phase inversion process, the better hydrophilicity of 5:5 membranes would help the diffusion of DMAc from polymer matrix into water, and thus facilitate the formation of bigger pore density [35]. With respect to cross-section structure, the pristine membranes presented a typical asymmetric structure consisting of a thin dense top-layer and a porous finger-like sub-layer. However, the modified membranes exhibited a strong change in the sub-layer morphology. For the PVDF/OMWCNTs or PVDF/GO membranes, it seemed that the finger-like microvoids turned to be elongated across the thickness, and became wider close to the back side of membranes. And for the PVDF/GO/OMWCNTs membranes, it was found that the bottom surface of the finger-like macrovoids increased, and became wider with strong separation of the dense top-layer. The homogeneous dispersion of GO and OMWCNTS in the casting solution (Fig. 2) may be expected to increase the affinity between the casting solution and precipitant, enhancing solvent–nonsolvent exchange and creating the conditions for instantaneous demixing and associated macrovoids formation [36]. Large macrovoids in the substructure typically can result in increased permeability [37]. Besides, comparing the upper side of the finger-like cavities in Fig. 4, the 5:5 (GO/OMWCNTs) membranes appeared larger and sparser in contrast with other membranes, which undoubtedly benefited the water permeability (Fig. 6) and diminished the membrane fouling resistance (Fig. 9) [34].

3.3.2. Contact angle of membranes

Contact angle measurements were widely used for the characterization of the hydrophilicity of membrane surfaces. And hydrophilicity is one of the most important properties of membranes, which could influence the flux and antifouling ability of membranes [29,38]. The pristine PVDF membranes have the highest initial contact angle of 78° from Fig. 5. Owing to the hydration effect between its carboxyl groups and water [39], after incorporation of hydrophilic low-dimensional carbon nanomaterials, the initial contact angles of modified membranes were all decreased. Furthermore, difference in the decaying rate of pristine membranes and modified membranes shows obviously enhanced water diffusing in 150 s determination, implying the better water affinity and improved hydrophilicity for modified membranes. Additionally, hydrophilicity increments of all PVDF/GO/OMWCNTs membranes are higher than those of PVDF/OMWCNTs or PVDF/GO membranes. Two factors were proposed to explain the synergetic effects of the mixture of GO and OMWCNTs: (I) flexible OMWCNTs can construct GO to form 3-D hybrid structure, which inhibits face to face aggregation of multi-graphene platelets. This results in a high contact area between the GO/OMWCNTs structures and the polymer matrix and (II) the better dispersion of hybrid materials making the oxygen-containing functional groups on the membrane surface play their role effectively [40]. As a result, the increased hydrophilicity will play a positive role in promoting membrane permeability and anti-fouling performance [36], which is discussed in detail in later part.

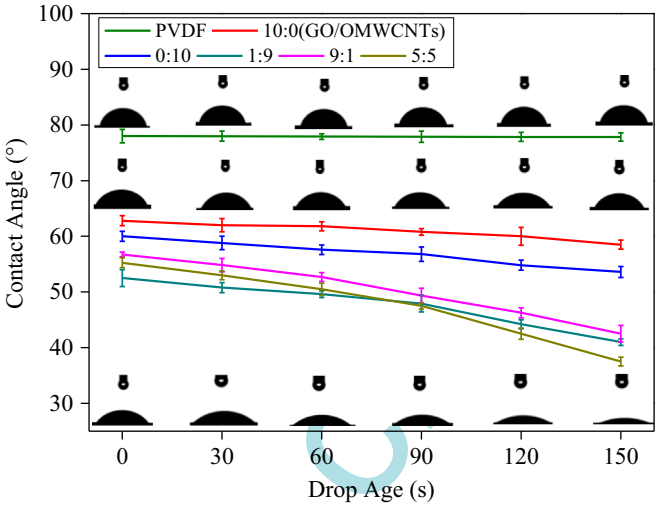

Fig. 5. Decay of water contact angle as a function of time and the photographs of water drops of PVDF, 10:0 and 5:5 membranes.

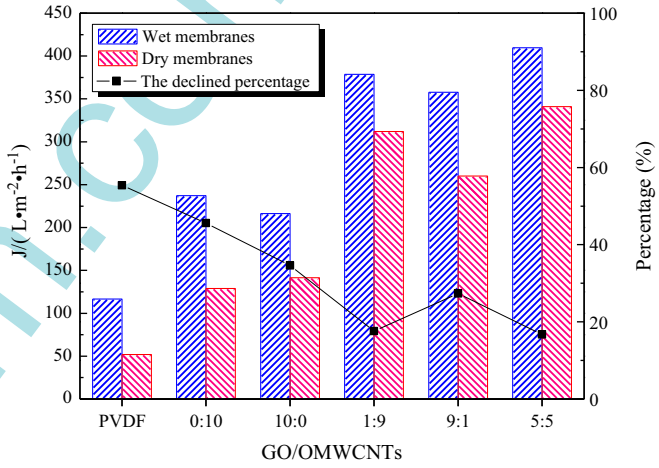

Fig. 6. Pure water flux of PVDF and modified membranes kept in different states and the declined percentage of dry membranes than wet membranes.

3.3.3. Pure water flux of wet and dry membranes

Flux measurements are a convenient method for obtaining information about the permeation performance of membranes. The pure water flux of different membranes is presented in Fig. 6. Compared with that of pristine PVDF membranes (116.5 L $m^{-2} h^{-1}$), the pure water flux of modified membranes was enhanced by 103.54% (GO/OMWCNTs=0:10), 85.68% (10:0), 224.94% (1:9), 207.09% (9:1) and 251.73% (5:5), respectively, which proved the fact that the oxidized low-dimensional carbon nanomaterials/PVDF membranes were successfully endowed with vital performance of permeation. In general, the pure water flux increases significantly as a consequence of hydrophilicty enhancement [39,41]. As we can see from Fig. 5, the fact is in agreement with the observed sequence of contact angle. Additionally, the improved percentage of pure water flux of PVDF/GO/OMWCNTs membranes is obviously higher than that of PVDF/OMWCNTs or PVDF/GO membranes, which results from the homogeneous dispersions of hybrid materials (Fig. 2). Considering the results in

Figs. 4 and 5, the improved water permeability of modified membranes might be due to various factors. Firstly, the modified membranes were all endowed with advantageous porous surface and favorable cross-section structure (Fig. 4), which definitely played a positive role in promoting membrane permeability [42]. Secondly, the addition of carbon nanomaterials resulted in the increase of membrane hydrophilicity (Fig. 5), which might also act favorably in promoting the water permeability.

Furthermore, we can see that the dried modified membranes still exhibit excellent permeability due to its spontaneous wettability, while the water flux of the dried pristine PVDF membranes dramatically decreases to 52 L m^{-2} h^{-1}, only 44% of that of wet PVDF membranes. Moreover, it is clear that the declined percentage of PVDF/OMWCNTs or PVDF/GO membranes is higher than that of PVDF/GO/OMWCNTs membranes. As a result, the incorporation of low-dimensional carbon materials provide the membranes with dry storage capability without sacrificing the permeability, which is favorable for keeping the membrane bacteria proof and for transportation.

3.4. Anti-fouling performance and mechanisms

3.4.1. Fouling mechanisms of membranes

The fouling mechanism of membranes provides a good understanding on the membrane capacity, defined as permeate volume per membrane area which can be processed until the flux declines to a certain fraction of the initial flux, or until the formed cake starts to increase the filtration resistance dramatically. It is well known that membrane fouling can be influenced by hydrodynamic conditions, such as permeation drag and back transport, and chemical interaction between foulants and membranes [43,44]. Since all the membranes were tested at the same hydrodynamic condition, the different fouling behaviors could be attributed to surface properties of the membranes which were changed by nanofiller entrapment. Based on the resistance-in-series model [22], the total resistance (R_{tot}) is the sum of the hydraulic resistance (R_m), cake layer resistance (R_g), concentration polarization resistance (R_c) and adsorption resistance (R_a) into membrane pores and walls. As apparent from Fig. 7(a), the R_g value ranging between 8.94×10^7 m^{-1} for pristine PVDF membranes and 0.69×10^7 m^{-1} for modified membranes with the ratio of 5:5 (GO/OMWCNTs) is much higher than the R_m, R_a and R_c value. The results suggest that the main fouling mechanism for all membranes was the cake layer formation. In addition, the R_g value of all modified membranes is lower than that of pristine PVDF membranes, which suggests that introducing the low-dimensional carbon nanofillers may decrease the adhesion or the adsorption of BSA on the membrane surface [44].

On the other hand, this is further supported by the R_g/R_{tot} ratio. As we can see from Fig. 7(b), the ratio decreased from 53.63% of the pristine PVDF to 17.6% of the modified membranes with the ratio of 5:5 (GO/OMWCNTs), which was attributable to the reduction in hydrophobic interaction between the membranes and BSA. The modified membranes can be more hydrophilic than the pristine PVDF membranes due to the higher affinity of carbon nanomaterials to water. Therefore, hydrophobic adsorption between BSA and modified membranes was reduced. And the adhesion effect is described in more detail below.

3.4.2. Interaction force between membrane surface and BSA-immobilized tip

Because fouling of the membranes originates from the accumulation of foulant on the membranes, the anti-fouling performance of the membranes is dominated by interaction between the foulant and the membrane surface. Adhesion force measurements by AFM are presented to support the antifouling mechanism of the membranes. And previous results demonstrated by others also have shown that the magnitude of the adhesion force correlates well with the fouling propensity of membranes and surfaces in the presence of organic foulants [45–49]. The influences of OMWCNTs, GO and GO/OMWCNTs on the corresponding intermolecular adhesion are presented in Fig. 8. Results suggest that the adhesion force between the model foulant (BSA) and the modified membranes should be weak, while between BSA and pristine PVDF membranes is strong. It will lead to an increase in the intermolecular adhesion between BSA molecules and, consequently, to a thicker and more compact fouling layer on the membrane surface. n detail, no measurements of adhesion force were made in excess of 1 nN of the modified membranes, while it is close to 2 nN for the pristine PVDF membranes. Furthermore, the decreased adhesion force of PVDF/GO/OMWCNTs membranes relative to the OMWCNTs-only or GO-only membranes is quite evident. It was in striking agreement with the fouling rate determined from fouling experiments (Fig. 7). Elimelech [50] has proved that the

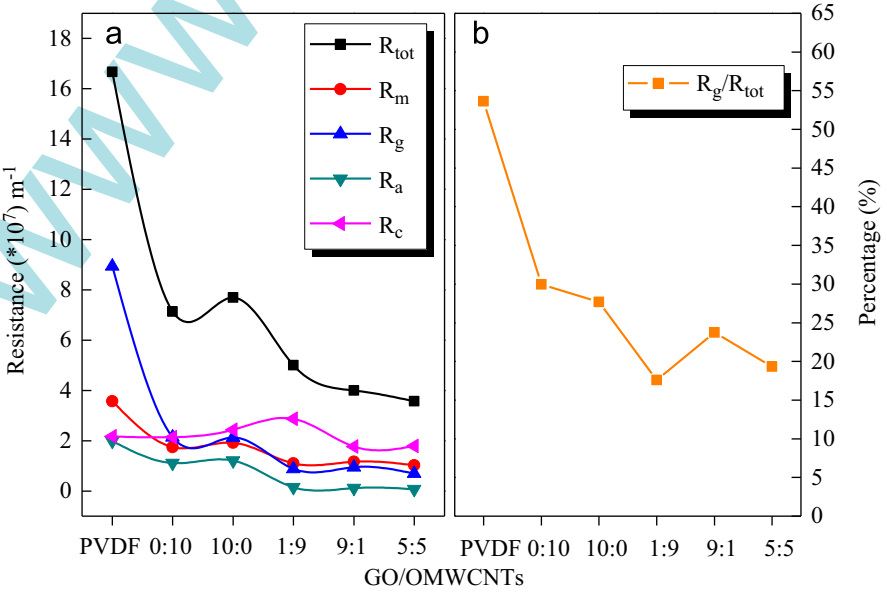

Fig. 7. Filtration resistance of pristine membranes and modified membranes.

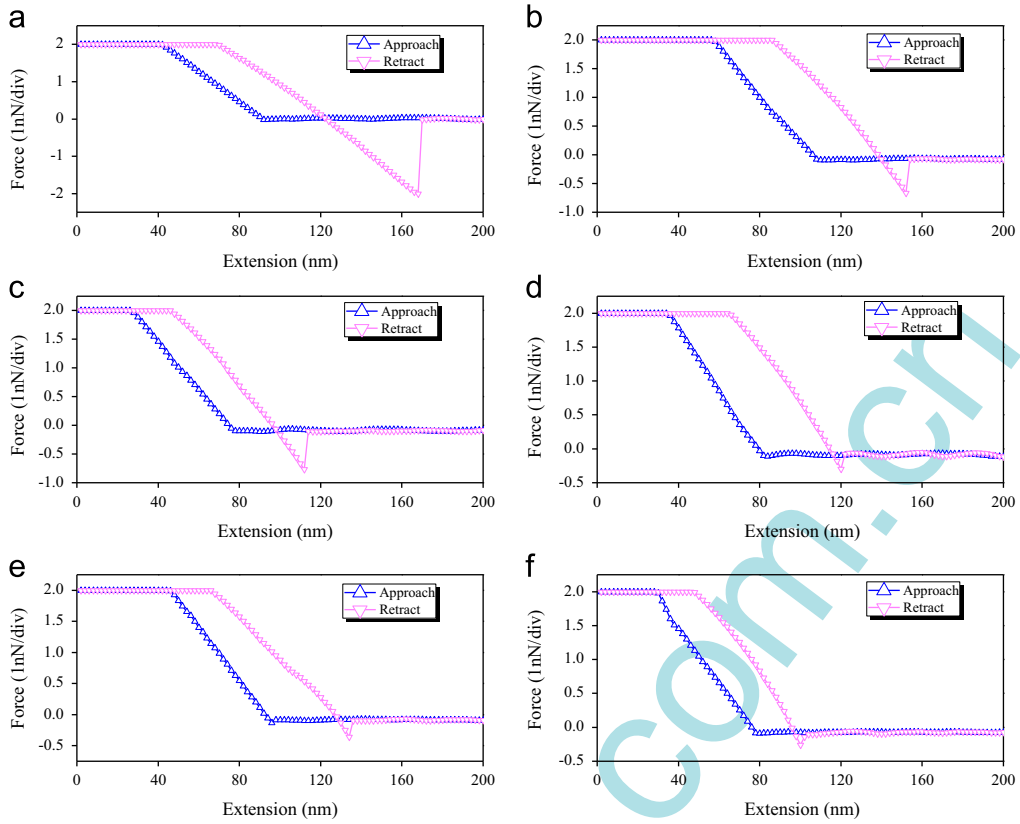

Fig. 8. Force–extension curves recorded with a BSA-immobilized tip against (a) pristine membranes, (b) 0:10 (GO/OMWCNTs), (c) 10:0, (d) 1:9, (e) 9:1 and (f) 5:5 membrane surfaces coated on silicon wafer.

significant adhesion force measured with BSA indicated the formation of a crossed-linked BSA gel layer during fouling through intermolecular bridging among BSA molecules, leading to more flux decline (Fig. 6). The agreement between the magnitude of interfacial forces and the observed rates of membrane fouling implies that interfacial force measurements between a BSA-immobilized tip and the membranes are directly related to the fouling potential of membranes. It also suggests that elimination of membrane–foulant adhesion is the key factor in controlling membrane organic fouling [51].

3.4.3. *Anti-fouling performance and mechanisms of membranes*

To investigate the filtration performance, the dead end filtration experiments were conducted. The effect of low-dimensional carbon materials on the BSA flux and the pure water flux (before and after BSA filtration) is shown in Fig. 9. The optimum parameter for comparing the anti-fouling characteristics of prepared membranes could be *FRR*. The value of the *FRR* for pristine PVDF membranes was calculated to be 34.64% and 13.68% at 60 min and 120 min, respectively, indicating that serious membrane fouling occurred due to BSA adsorption, which is consistent with the AFM characterization. The main reason of the fouling is trapping and aggregation of the foulants in the membrane pores and "valleys" of the surface to form the thick fouling layer [52] (Fig. 10(a)) which do not considerably detach from membrane surface by cleaning process. All of the modified membranes showed the higher *FRR* compared with the pristine PVDF membranes and the *FRR* of the membranes with the ratio of 5:5(GO/OMWCNTs) even amount to 98.28%. It is deduced from the fact that the modified membranes are well tailored by nanomaterials and they enhanced the hydrophilicity (Fig. 5) of all modified membranes and thus improved the anti-fouling performance remarkably [53].

We have known that the irreversible fouling dominates the total fouling because the DR_{ir} describes the fouling caused by adsorption or deposition of protein molecules on the membrane surface [29]. As we can see from Fig. 9, it is obvious that the pristine PVDF membranes had highest DR_{ir} (70.36%, about 82.23% of total fouling) due to the lower surface hydrophilicity [54]. Therefore, hydrophobic adsorption between BSA and pristine PVDF membranes was strong [55]. And all PVDF/GO/OMWCNTs composite membranes exhibit lower DR_{ir} than PVDF/OMWCNTs or PVDF/GO membranes. The order of anti-fouling performance is in agreement with the variation characteristics of the pure water flux, intermolecular adhesion force and the structure of the cake layer as shown in Figs. 6, 8 and 10. It seems that, the higher the adhesion force of the membrane – foulant, the more compact the corresponding structure's cake layer and the lower pure water flux and anti-fouling performance. On the contrary, a lower adhesion force of membrane – foulant will result in a looser cake layer and a higher pure water flux and anti-fouling performance. Results revealed that the membrane – foulant adhesion force should be a good indicator of pure water flux and cake layer structure of the membranes. Additionally, some reasons can explain the synergetic effects of the mixture of GO and OMWCNTs. The long and tortuous OMWCNTs can construct hierarchical GO/OMWCNTs architecture to inhibit the stacking of GO resulting in good dispersion of GO/OMWCNTs on the membrane surface and in the PVDF matrix. Hence, the improved anti-fouling performance is mainly because the GO/OMWCNTs enhanced the surface hydrophilicity, which lowers its interaction with BSA [53]. And the GO/OMWCNTs can bind a greater quantity of free water, which could prevent the protein molecules from contacting with the membrane surface tightly and reduce the protein adsorption [56]. Less protein adsorption at the membrane surface makes it easier to be cleaned. Taking this factor into consideration, the incorporated

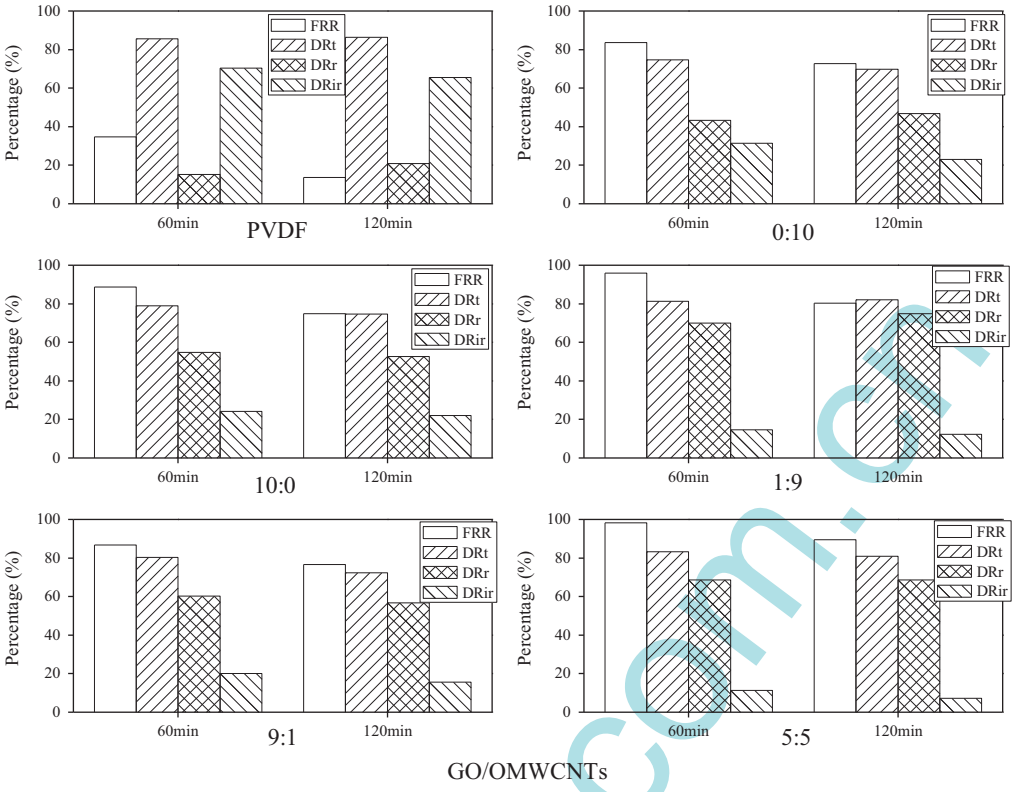

Fig. 9. Time dependence of water permeation flux variations during membrane filtration.

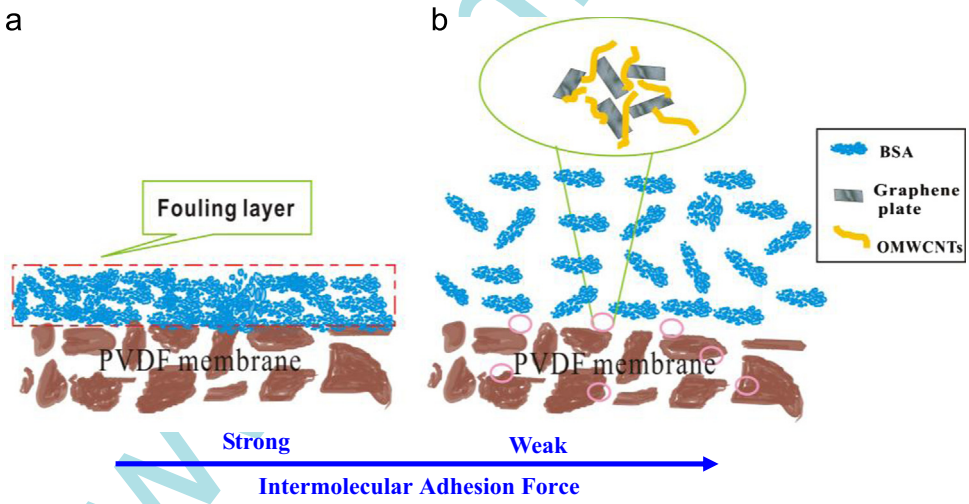

Fig. 10. Schematic illustration of anti-fouling mechanisms of (a) pristine membranes and (b) modified membranes.

GO/OMWCNTs improve the anti-fouling performance of membranes considerably. Among all the modified membranes, the ratio of 5:5 (GO/OMWCNTs) was deemed to be the optimum load, despite a similar fouling rate observed for all GO/OMWCNTs loads, as it possesses higher pure water flux and steady-state permeability, and lower fouling rate, lower R_g as well as higher *FRR* value compared with other tested modified membranes.

3.4.4. Adhesion between carbon nanomaterials and membranes

The effect of carbon nanomaterials should be determined not only from the point of view of fouling mitigation and water sustainability, but also from the potential stability determined by whether the carbon nanomaterials are released to the environment or not [57]. Because a principal method of cleaning membranes in filtration facilities is periodic backwashing of the membranes, the carbon nanomaterials must have a strong adhesive force to the membrane, or they will be removed during backwashing. Haiou Huang etc. [10] have investigated the adhesion properties of the carbon nanotubes to membranes by backwashing experiments. In our study, different membranes in the syringe-driven filter were also flushed several times by the pure water which was stored in a 20 ml syringe during the filtration run at a roughly constant flow rate. And images of different membranes before and after backwashing were shown in Fig. 11. It can be clearly seen that the adhesive force was strong between the carbon nanomaterials and the modified membranes as images looked the same before and after backwashing. Additionally, in

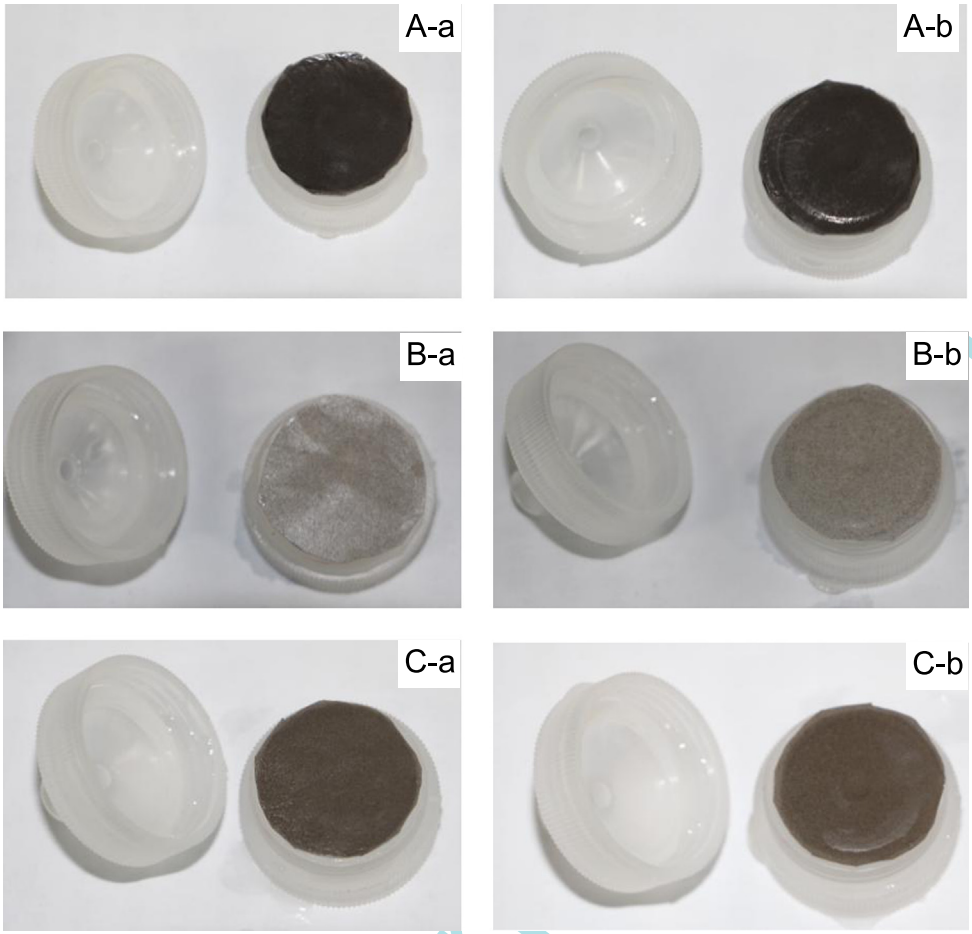

Fig. 11. (a) Before backwashing and (b) after backwashing images of (A) 0:10 (GO/OMWCNTs), (B) 10:0 and (C) 5:5 membranes.

Table 1
The contact angles of different membranes before and after backwashing.

Membranes (GO/OMWCNTs)	Contact angle (°)	
	Before backwashing	After backwashing
0:10	59.8 ± 0.3	59.6 ± 0.5
10:0	62.5 ± 0.2	62.8 ± 0.4
5:5	55.0 ± 0.5	55.2 ± 0.2

order to verify the results exactly, the contact angles of membranes before and after backwashing were also measured and the results were indicated in Table 1. It demonstrated that there was no change in the measured contact angles of all membranes, which was well consistent with the backwashing images (Fig. 11). As a whole, both the backwashing experiments and measured contact angle results illustrated that the membranes modified by carbon nanomaterials are very hopeful for the water treatment system. Besides that, more experimental studies are still required to investigate in order to bring a new insight into a wider application of carbon nanomaterials-based membranes in practical industry.

4. Conclusions

In conclusion, we have demonstrated the feasibility of designing a new generation of composite ultrafiltration membranes for investigating fouling control and anti-fouling mechanism based on the synergistic behavior of GO/OMWCNTs nanofiller. Major findings from this study are as follows:

(1) UV–vis spectra and zeta potential validated that the mixture of GO/OMWCNTs showed better dispersion than either of that, which was beneficial to the permeability and anti-fouling performance of membranes.
(2) The pure water flux of membranes with the ratio of 0:10 (GO/OMWCNTs), 10:0, 1:9, 9:1 and 5:5 was increased by 103.54%, 85.68%, 224.94%, 207.09% and 251.73%, respectively, compared with those of pristine PVDF membranes. The contact angle of pristine PVDF membranes almost remains stable during the drop aging (78°–77.82°), while it is remarkably decreasing for PVDF/OMWCNTs membranes (62.8°–58.5°) and PVDF/GO membranes(60°–53.6°), and the membranes with the ratio of 5:5 even amount to 37.5° at 150 s determination. Furthermore, the improved pore density of modified membranes, as indicated by SEM tests, probably made much contribution to the enhancement of permeation performance.
(3) For the PVDF and modified membranes, cake formation is the predominant fouling mechanism with a direct statistical correlation between membrane total resistance (R_{tot}) and cake resistance (R_g).
(4) Interaction force measurements between the membranes and an AFM BSA-immobilized tip provided valuable information about the antifouling mechanisms of the membranes. And the force measurements suggest that the anti-fouling performance of the modified membranes is attributable to the affinity of oxidized low-dimensional carbon nanomaterials with water, creating an energetic barrier to the adsorption of BSA.

(5) The membranes entrapped by low-dimensional carbon nanomaterials showed lower flux decline compared with pristine PVDF membranes, and the *FRR* of membranes with the ratio of (GO/OMWCNTs) 5:5 even achieved 98.5%, indicating a better synergetic effect of OMWCNTs and GO. It is also concluded that the increase of BSA in the fouling layer of pristine PVDF membranes would have a negative effect on the anti-fouling performance.

Overall, it can be concluded that minimizing the stacking effect and aggregation of low-dimensional carbon nanomaterials are the most important issue to resolve on account of the potential application for carbon nanomaterial-based composite membranes. Consequently, combining OMWCNTs and GO will become a very important concept for improving performance of PVDF composite membranes.

Acknowledgments

The work was funded by the National Natural Science Foundation of China (11175130), Natural Science Foundation of Tianjin, China (10JCYBJC02300), China Postdoctoral Science Foundation (2012M520578) and the Jiangsu Planned Projects for Postdoctoral Research Funds (1202067C).

Nomenclature

A	effective area of membranes (m^2)
AFM	atomic force microscope
BSA	bovine serum albumin
CA	contact angle (°)
DMAc	N, N-dimethylacetamide
DR_{ir}	irreversible flux decline ratio
DR_r	reversible flux decline ratio
DR_t	total flux decline ratio
FRR	flux recovery ratio
FTIR	Fourier-Transform Infrared spectroscopy
GO	graphene oxide
J	pure water flux ($L\,m^{-2}\,h^{-1}$)
J_{irr}	pure water flux after cleaning membranes ($L\,m^{-2}\,h^{-1}$)
J_{mem}	pure water flux through a clean membrane ($L\,m^{-2}\,h^{-1}$)
J_p	BSA flux ($L\,m^{-2}\,h^{-1}$)
J_{pore}	pure water flux after BSA permeation ($L\,m^{-2}\,h^{-1}$)
J_{tot}	permeate flux of BSA after pure water flux ($L\,m^{-2}\,h^{-1}$)
$J_{w,120}$	after-washing pure water flux at 120 min ($L\,m^{-2}\,h^{-1}$)
$J_{w,60}$	after-washing pure water flux at 60 min ($L\,m^{-2}\,h^{-1}$)
J_w	initial pure water flux ($L\,m^{-2}\,h^{-1}$)
OMWCNTs	oxidized carbon nanotubes
PBS	phosphate buffer solution
PVDF	polyvinylidene fluoride
PVP	polyvinyl pyrrolidone
R_a	adsorption resistance
R_c	concentration polarization resistance
R_g	cake layer resistance
R_m	hydraulic resistance
R_{tot}	total filtration resistance
SEM	scanning electron microscopy
T	permeation time (h)
TMP	transmembrane pressure (Mpa)
UV–vis	ultraviolet–visible
μ	viscosity of pure water (Pa s)

References

[1] K. Xiao, X. Wang, X. Huang, T.D. Waite, X. Wen, Combined effect of membrane and foulant hydrophobicity and surface charge on adsorptive fouling during microfiltration, Journal of Membrane Science 373 (2011) 140–151.
[2] M. Tao, F. Liu, L. Xue, Hydrophilic poly(vinylidene fluoride) (PVDF) membrane by in situ polymerisation of 2-hydroxyethyl methacrylate (HEMA) and microphase separation, Journal of Materials Chemistry 22 (2012) 9131–9137.
[3] S.J. Lee, M. Dilaver, P.-K. Park, J.H. Kim, Comparative analysis of fouling characteristics of ceramic and polymeric microfiltration membranes using filtration models, Journal of Membrane Science 432 (2013) 97–105.
[4] A. Akthakul, R.F. Salinaro, A.M. Mayes, Antifouling polymer membranes with subnanometer size selectivity, Macromolecules 37 (2004) 7663–7668.
[5] R. Naim, A.F. Ismail, A. Mansourizadeh, Effect of non-solvent additives on the structure and performance of PVDF hollow fiber membrane contactor for CO_2 stripping, Journal of Membrane Science 423 (2012) 503–513.
[6] Y. Chang, C.Y. Ko, Y.J. Shih, D. Quemener, A. Deratani, T.C. Wei, D.M. Wang, J.Y. Lai, Surface grafting control of PEGylated poly(vinylidene fluoride) antifouling membrane via surface-initiated radical graft copolymerization, Journal of Membrane Science 345 (2009) 160–169.
[7] X.X. Yang, B.W. Zhang, Z.Y. Liu, B. Deng, M. Yu, L.F. Li, H.Q. Jiang, J.Y. Li, Preparation of the antifouling microfiltration membranes from poly(N,N-dimethylacrylamide) grafted poly(vinylidene fluoride) (PVDF) powder, Journal of Materials Chemistry 21 (2011) 11908–11915.
[8] A. Tiraferri, Y. Kang, E.P. Giannelis, M. Elimelech, Superhydrophilic thin-film composite forward osmosis membranes for organic fouling control: fouling behavior and antifouling mechanisms, Environmental Science and Technology 46 (2012) 11135–11144.
[9] V. Vatanpour, S.S. Madaeni, R. Moradian, S. Zinadini, B. Astinchap, Fabrication and characterization of novel antifouling nanofiltration membrane prepared from oxidized multiwalled carbon nanotube/polyethersulfone nanocomposite, Journal of Membrane Science 375 (2011) 284–294.
[10] G.S. Ajmani, D. Goodwin, K. Marsh, D.H. Fairbrother, K.J. Schwab, J.G. Jacangelo, H. Huang, Modification of low pressure membranes with carbon nanotube layers for fouling control, Water Research 46 (2012) 5645–5654.
[11] N. Wang, S. Ji, G. Zhang, J. Li, L. Wang, Self-assembly of graphene oxide and polyelectrolyte complex nanohybrid membranes for nanofiltration and pervaporation, Chemical Engineering Journal 213 (2012) 318–329.
[12] Y. Zhao, Z. Xu, M. Shan, C. Min, B. Zhou, Y. Li, B. Li, L. Liu, X. Qian, Effect of graphite oxide and multi-walled carbon nanotubes on the microstructure and performance of PVDF membranes, Separation and Purification Technology 103 (2013) 78–83.
[13] J. Zhang, Z. Xu, W. Mai, C. Min, B. Zhou, M. Shan, Y. Li, C. Yang, Z. Wang, X. Qian, Improved hydrophilicity, permeability, antifouling and mechanical performance of PVDF composite ultrafiltration membranes tailored by oxidized low-dimensional carbon nanomaterials, Journal of Materials Chemistry A 1 (2013) 3101–3111.
[14] S. Wang, R. Liang, B. Wang, C. Zhang, Dispersion and thermal conductivity of carbon nanotube composites, Carbon 47 (2009) 53–57.
[15] Y. Si, E.T. Samulski, Exfoliated graphene separated by platinum nanoparticles, Chemistry of Materials 20 (2008) 6792–6797.
[16] D. Li, M.B. Mueller, S. Gilje, R.B. Kaner, G.G. Wallace, Processable aqueous dispersions of graphene nanosheets, Nature Nanotechnology 3 (2008) 101–105.
[17] S. Chatterjee, F. Nafezarefi, N.H. Tai, L. Schlagenhauf, F.A. Nueesch, B.T.T. Chu, Size and synergy effects of nanofiller hybrids including graphene nanoplatelets and carbon nanotubes in mechanical properties of epoxy composites, Carbon 50 (2012) 5380–5386.
[18] K.A. Wepasnick, B.A. Smith, K.E. Schrote, H.K. Wilson, S.R. Diegelmann, D.H. Fairbrother, Surface and structural characterization of multi-walled carbon nanotubes following different oxidative treatments, Carbon 49 (2011) 24–36.
[19] D.C. Marcano, D.V. Kosynkin, J.M. Berlin, A. Sinitskii, Z. Sun, A. Slesarev, L.B. Alemany, W. Lu, J.M. Tour, Improved synthesis of graphene oxide, ACS Nano 4 (2010) 4806–4814.
[20] E.C. Cho, D.H. Kim, K. Cho, Contact angles of oils on solid substrates in aqueous media: correlation with AFM data on protein adhesion, Langmuir 24 (2008) 9974–9978.
[21] W.S. Ang, A. Tiraferri, K.L. Chen, M. Elimelech, Fouling and cleaning of RO membranes fouled by mixtures of organic foulants simulating wastewater effluent, Journal of Membrane Science 376 (2011) 196–206.
[22] R.S. Juang, H.L. Chen, Y.S. Chen, Membrane fouling and resistance analysis in dead-end ultrafiltration of Bacillus subtilis fermentation broths, Separation and Purification Technology 63 (2008) 531–538.
[23] J. Shen, Y. Hu, M. Shi, X. Lu, C. Qin, C. Li, M. Ye, Fast and facile preparation of graphene oxide and reduced graphene oxide nanoplatelets, Chemistry of Materials 21 (2009) 3514–3520.

[24] Z. Wang, Q. Liu, H. Zhu, H. Liu, Y. Chen, M. Yang, Dispersing multi-walled carbon nanotubes with water–soluble block copolymers and their use as supports for metal nanoparticles, Carbon 45 (2007) 285–292.
[25] K.R. Reddy, B.C. Sin, K.S. Ryu, J.C. Kim, H. Chung, Y. Lee, Conducting polymer functionalized multi-walled carbon nanotubes with noble metal nanoparticles: synthesis, morphological characteristics and electrical properties, Synthetic Metals 159 (2009) 595–603.
[26] S.H. Aboutalebi, A.T. Chidembo, M. Salari, K. Konstantinov, D. Wexler, H.K. Liu, S.X. Dou, Comparison of GO, GO/MWCNTs composite and MWCNTs as potential electrode materials for supercapacitors, Energy and Environmental Science 4 (2011) 1855–1865.
[27] F.M. van der Kooij, H.N.W. Lekkerkerker, Formation of nematic liquid crystals in suspensions of hard colloidal platelets, Journal of Physical Chemistry B 102 (1998) 7829–7832.
[28] K.B. Male, E. Lam, J. Montes, J.H.T. Luong, Noninvasive cell-based impedance spectroscopy for real-time probing inhibitory effects of graphene derivatives, ACS Applied Materials and Interfaces 4 (2012) 3643–3649.
[29] V. Vatanpour, S.S. Madaeni, L. Rajabi, S. Zinadini, A.A. Derakhshan, Boehmite nanoparticles as a new nanofiller for preparation of antifouling mixed matrix membranes, Journal of Membrane Science 401 (2012) 132–143.
[30] H. Wu, B. Tang, P. Wu, ANTI Novel ultrafiltration membranes prepared from a multi-walled carbon nanotubes/polymer composite, Journal of Membrane Science 362 (2010) 374–383.
[31] E. Celik, H. Park, H. Choi, Carbon nanotube blended polyethersulfone membranes for fouling control in water treatment, Water Research 45 (2011) 274–282.
[32] Y. Mansourpanah, E.M. Habili, Preparation and modification of thin film PA membranes with improved antifouling property using acrylic acid and UV irradiation, Journal of Membrane Science 430 (2013) 158–166.
[33] S.B. Teli, S. Molina, E.G. Calvo, A.E. LozanoJ. de Abajo, Preparation, characterization and antifouling property of polyethersulfone-PANI/PMA ultrafiltration membranes, Desalination 299 (2012) 113–122.
[34] S. Liang, K. Xiao, Y. Mo, X. Huang, A novel ZnO nanoparticle blended polyvinylidene fluoride membrane for anti-irreversible fouling, Journal of Membrane Science394–395 (2012) 184–192.
[35] B. Deng, M. Yu, X. Yang, B. Zhang, L. Li, L. Xie, J. Li, X. Lu, Antifouling microfiltration membranes prepared from acrylic acid or methacrylic acid grafted poly(vinylidene fluoride) powder synthesized via pre-irradiation induced graft polymerization, Journal of Membrane Science 350 (2010) 252–258.
[36] Y. Sui, Z.N. Wang, X.L. Gao, C.J. Gao, Antifouling PVDF ultrafiltration membranes incorporating PVDF-g-PHEMA additive via atom transfer radical graft polymerizations, Journal of Membrane Science 413 (2012) 38–47.
[37] J.F. Hester, P. Banerjee, Y.Y. Won, A. Akthakul, M.H. Acar, A.M. Mayes, ATRP of amphiphilic graft copolymers based on PVDF and their use as membrane additives, Macromolecules 35 (2002) 7652–7661.
[38] Z. Yi, L.P. Zhu, Y.Y. Xu, Y.F. Zhao, X.T. Ma, B.K. Zhu, Polysulfone-based amphiphilic polymer for hydrophilicity and fouling-resistant modification of polyethersulfone membranes, Journal of Membrane Science 365 (2010) 25–33.
[39] J. Maria Arsuaga, A. Sotto, G. del Rosario, A. Martinez, S. Molina, S.B. TeliJ. de Abajo, Influence of the type, size, and distribution of metal oxide particles on the properties of nanocomposite ultrafiltration membranes, Journal of Membrane Science 428 (2013) 131–141.
[40] S.-Y. Yang, W.-N. Lin, Y.-L. Huang, H.-W. Tien, J.-Y. Wang, C.-C.M. Ma, S.-M. Li, Y.-S. Wang, Synergetic effects of graphene platelets and carbon nanotubes on the mechanical and thermal properties of epoxy composites, Carbon 49 (2011) 793–803.
[41] F. Zhang, W. Zhang, Y. Yu, B. Deng, J. Li, J. Jin, Sol–gel preparation of PAA-g-PVDF/TiO2 nanocomposite hollow fiber membranes with extremely high water flux and improved antifouling property, Journal of Membrane Science 432 (2013) 25–32.
[42] P. van der Marel, A. Zwijnenburg, A. Kemperman, M. Wessling, H. Temmink, W. van der Meer, Influence of membrane properties on fouling in submerged membrane bioreactors, Journal of Membrane Science 348 (2010) 66–74.
[43] W. Lee, S. Kang, H. Shin, Sludge characteristics and their contribution to microfiltration in submerged membrane bioreactors, Journal of Membrane Science 216 (2003) 217–227.
[44] N. Maximous, G. Nakhla, W. Wan, K. Wong, Performance of a novel ZrO_2/PES membrane for wastewater filtration, Journal of Membrane Science 352 (2010) 222–230.
[45] D.-G. Kim, H. Kang, S. Han, J.-C. Lee, The increase of antifouling properties of ultrafiltration membrane coated by star-shaped polymers, Journal of Materials Chemistry 22 (2012) 8654–8661.
[46] Y. Mo, A. Tiraferri, N.Y. Yip, A. Adout, X. Huang, M. Elimelech, Improved antifouling properties of polyamide nanofiltration membranes by reducing the density of surface carboxyl groups, Environmental Science and Technology 46 (2012) 13253–13261.
[47] C.J. Weinman, N. Gunari, S. Krishnan, R. Dong, M.Y. Paik, K.E. Sohn, G.C. Walker, E.J. Kramer, D.A. Fischer, C.K. Ober, Protein adsorption resistance of antibiofouling block copolymers containing amphiphilic side chains, Soft Matter 6 (2010) 3237–3243.
[48] S. Kang, A. Asatekin, A.M. Mayes, M. Elimelech, Protein antifouling mechanisms of PAN UF membranes incorporating PAN-g-PEO additive, Journal of Membrane Science 296 (2007) 42–50.
[49] A. Asatekin, S. Kang, M. Elimelech, A.M. Mayes, Anti-fouling ultrafiltration membranes containing polyacrylonitrile-graft-poly (ethylene oxide) comb copolymer additives, Journal of Membrane Science 298 (2007) 136–146.
[50] S. Lee, M. Elimelech, Relating organic fouling of reverse osmosis membranes to intermolecular adhesion forces, Environmental Science and Technology 40 (2006) 980–987.
[51] W.-Z. Yu, N. Graham, H.-J. Liu, H. Li, J.-H. Qu, Membrane fouling by Fe-Humic cake layers in nano-scale: effect of in-situ formed Fe in-situ formed Fe(III) coagulant, Journal of Membrane Science 431 (2013) 47–54.
[52] J. Pieracci, J.V. Crivello, G. Belfort, Increasing membrane permeability of UV-modified poly(ether sulfone) ultrafiltration membranes, Journal of Membrane Science 202 (2002) 1–16.
[53] Q.-F. An, W.-D. Sun, Q. Zhao, Y.-L. Ji, C.-J. Gao, Study on a novel nanofiltration membrane prepared by interfacial polymerization with zwitterionic amine monomers, Journal of Membrane Science 431 (2013) 171–179.
[54] Y.-L. Ji, Q.-F. An, Q. Zhao, W.-D. Sun, K.-R. Lee, H.-L. Chen, C.-J. Gao, Novel composite nanofiltration membranes containing zwitterions with high permeate flux and improved anti-fouling performance, Journal of Membrane Science 390 (2012) 243–253.
[55] Q. Li, Q.-y. Bi, H.-H. Lin, L.-X. Bian, X.-L. Wang, A novel ultrafiltration (UF) membrane with controllable selectivity for protein separation, Journal of Membrane Science 427 (2013) 155–167.
[56] K. Ishihara, H. Nomura, T. Mihara, K. Kurita, Y. Iwasaki, N. Nakabayashi, Why do phospholipid polymers reduce protein adsorption? Journal of Biomedical Materials Research 39 (1998) 323–330.
[57] J. Kim, B. Van der Bruggen, The use of nanoparticles in polymeric and ceramic membrane structures: review of manufacturing procedures and performance improvement for water treatment, Environmental Pollution 158 (2010) 2335–2349.